Journal of Applied Fluid Mechanics, Vol. 17, No. 3, pp. 646-657, 2024.
Available online at www.jafmonline.net, ISSN 1735-3572, EISSN 1735-3645.
https://doi.org/10.47176/jafm.17.3.2181

Research on the Unsteady Flow and Vortex Characteristics of Cavitation at the Tongue in Centrifugal Pump

Z. Y. Luo[1], Y. Feng[1†], X. Y. Sun[1], Y. Gong[2], J. X. Lu[2] and X. W. Zhang[3]

[1] *Chengdu Fluid Dynamics Innovation Center, Chengdu, 610071, China*
[2] *Key Laboratory of Fluid and Power Machinery, Ministry of Education, Xihua University, Chengdu, 610039, China*
[3] *College of Energy and Power Engineering, Lanzhou University of Technology, Lanzhou, 730050, China*

†*Corresponding Author Email: fengyi0218@163.com*

ABSTRACT

In order to study the unsteady flow and vortex characteristics of tongue cavitation, numerical calculation is carried out for the whole flow channel given different conditions. Then, the calculation results are verified experimentally. The results show that after the occurrence of tongue cavitation in the centrifugal pump, it deteriorates with the decrease of $NPSH_a$. However, when $NPSH_a$ is reduced to 3.78 m, it does not change significantly anymore with the decrease of $NPSH_a$. The extrusion of fluid by the vapor at the tongue promotes the formation of the separation vortex, and the re-jet flow caused by the separation vortex leads to vapor shedding. The frequency of cavitation shedding is consistent with the frequency of vortex shedding. In the vorticity transport equation, the relative vortex stretching term and the relative vortex dilatation term dominate the vapor shedding by controlling the change in vorticity. The baroclinic torque term mainly affects the change of vorticity at the vapor-liquid interface, but to a much lesser extent than the first two terms.

Article History

Received July 22, 2023
Revised November 2, 2023
Accepted November 12, 2023
Available online January 1, 2024

Keywords:

Centrifugal pump
Tongue cavitation
Vortex
Vorticity transport equation
Stability

1. INTRODUCTION

Pumps play a pivotal role as fluid machine in a wide range of applications, including marine, aerospace, weaponry and health care (Lu et al., 2020; Al-Obaidi & Alhamid, 2023). Centrifugal pumps are used in 75% of all pump products (Liu, 2021) and about 20% of electricity is consumed by centrifugal pumps worldwide (Mandhare et al., 2019). However, cavitation has a serious impact on the safety and stability of pump operation. Cavitation in centrifugal pumps not only destabilizes the internal flow of the pump, resulting in a decrease in hydraulic performance, but it also induce vibration and noise. More seriously, it causes material damage (Shi et al., 2016; Jiang et al., 2019; Al-Obaidi, 2023b). Cavitating flow entails the highly complex interactions between microscopic cavitation and the macroscopic flow (Folden & Aschmoneit, 2023). A large number of researchers have studied the cavitation flow in pumps. AI-Obaidi and Qubian (2022) used the developed CFD code to perform transient numerical calculations of the flow field in a centrifugal pump with different diameters of the outlet impeller under single-phase and cavitation conditions. The findings reveal that the CFD model correctly simulates the centrifugal pump's performance and features. The study of cavitation-induced vibration and noise signals for in-pump flow monitoring and fault diagnosis has also attracted the interest of many researchers (Al-Obaidi, 2019, 2023a; Lu et al., 2023).

The leading edge of the blade is where centrifugal pumps are mainly concentrated in the cavitation of the original position (Tan et al., 2014). The flow separation marked by vortex instability shedding can happen close to this point (Hattori & Kishimoto, 2008). In order to meet the needs of different situations, centrifugal pumps often operate under the conditions that deviate from their design. When operating at high flow rates, cavitation may have been observed to occur initially at the volute tongue rather than the impeller (Bachert et al., 2010). The cavitation structure at the tongue is similar to the structure of shear turbulence vortex cavitation that occurs on the hydrofoil in the water tunnel (Dular et al., 2005). It has been demonstrated that the sheet cavities in the hydrofoil periodically break up and roll up into the clouds of cavitation (Astolfi et al., 2000). Foeth et al. (2006) and Foeth et al. (2008) used PIV and high-speed cameras to study the development of cavitation on the hydrofoils with different angles of attack, revealing that the shedding of the cavity is controlled by the direction and momentum of the re-entry jet and its impact on the free surface of the cavity. Ji et al. (2013), Park and Rhee (2013) confirmed the idea by performing numerical calculations. The

experimental study conducted by Pham et al. (1999) shows that the frequency of re-entry jet surge is equal to that of cavitation cloud shedding, while the analysis of gravity effect shows that the periodic shedding of cavitation cloud is affected by re-entry jet more than interface instability. Therefore, it can be assumed that cavitation cloud shedding is mainly driven by re-entry jet. Through experimental observation of cavitation flow around the NACA0015 hydrofoil, Kravtsova et al. (2014) found out that the flow at the leading edge of the hydrofoil determines the onset of cavitation, but the subsequent flow is substantially governed by the state of cavitation and significantly different from the flow in the absence of cavitation. There is still a clear distinction between tongue cavitation and hydrofoil cavitation. In the case of a single hydrofoil, the dynamics of cavitation is dominated by the periodic generation of self-excited cloud, the frequency of which is related to the velocity of flow and the Strouhal number (Dular & Bachert, 2009). The periodic variation of tongue cavitation is induced by a combination of pressure gradients on both sides of the blade and blade wake (Bachert et al., 2010). In engineering works, the pump head is often reduced by 3% of the $NPSH_a$ as the $NPSH_c$ of the pump operating flow (Lu, 2017). Hu et al. (2021) showed through visualization that at a high flow rate, no cavitation was found in the impeller when the pump head dropped by 3%. However, significant cavitation had occurred at the tongue. At the same time, the cavitation of the tongue can cause harm to the downstream wall (Xue, 2012). Lu et al. (2022) found out that the tongue cavitation is a vortex cavitation by numerically calculating the internal flow of the pump operating under the condition of overload. Xue and Piao (2012) used numerical calculations to determine the shedding mechanism of tongue cavitation. Hu et al.'s (2020) experiments verified the findings.

The existing research on the cavitation characteristics of centrifugal pumps is focused mostly on the cavitation occurring within the impeller, with only a small number of numerical calculations and visual experimental studies focusing on the characteristics of cavitation flow at the tongue. Though these studies have revealed some basic properties of tongue cavitation, they are far from comprehensive and insightful for the field of unsteady cavitation flow. In this research, the transient flow characteristics of the tongue cavitation are obtained by numerical calculation. Also, the vorticity transport equation is introduced to analyze the relationship between vorticity distribution and the development of tongue cavitation.

2. NUMERICAL CALCULATION

2.1 Numerical Model

The software CFX was applied to simulate the internal unsteady flow of the pump during operation. A water model of the pump was established by using the 3D modeling software UG, while both ends of the centrifugal pump were obtained with suitable extensions to prevent the effect of boundary conditions on the flow, as shown in Fig. 1. ICEM CFD was used to perform hexahedral

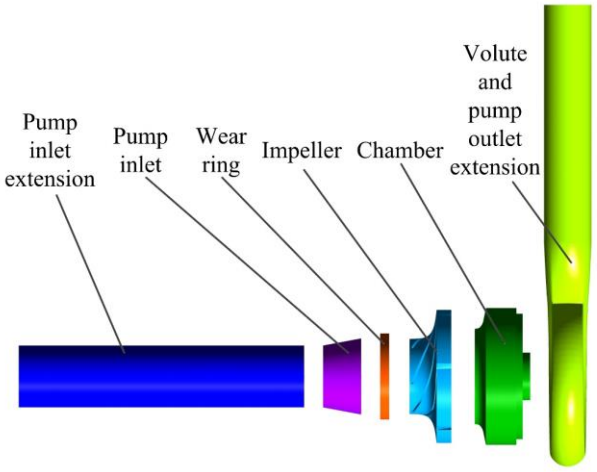

Fig. 1 Three-dimensional water model of centrifugal pump

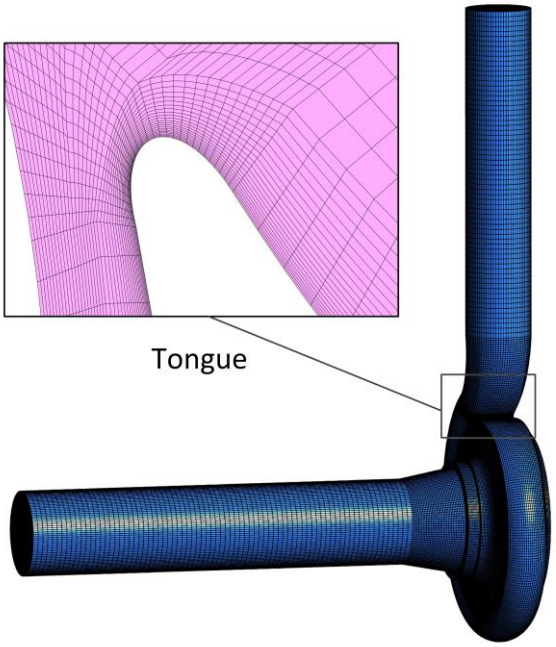

Fig. 2 Computational domain grid

structural meshing of all pump components. As shown in Fig. 2, the grid in the region close to the wall was encrypted. The total elements is 2.52×10^6, and the evaluation of grid quality is above 0.4. The grid independence verification and more information about the mesh parameters are presented in a previous study (Lu et al., 2019).

Because of the strong shear turbulence and flow separation at the tongue, the SST $k-\omega$ model (Launder & Spalding, 1974) was chosen as the turbulence model, which took turbulent shear stress transport into account. This turbulence model's ability to properly forecast the degree of fluid separation in the context of negative pressure gradients without overestimating eddy viscosity is its most significant feature (Si et al., 2014).

The Zwart-Gerber-Belamri model based on the simplified Rayleigh-Plesset equation is adopted in this study. This model ignores terms such as bubble surface

tension and viscosity while using the density and radius of the bubble to describe the vapor volume fraction. For simulating cavitation flow, it is the most widely used cavitation model (Yuan et al., 2018). Also, it has been experimentally verified by different researchers as suitable for simulating various cavitation flows (Bakir et al., 2004; Zhou et al., 2023). The Zwart-Gerber-Belamri model expression is illustrated below (Bakir et al., 2004):

$$R_e = F_{vap}\frac{3\alpha_{ruc}(1-\alpha_v)\rho_g}{R_B}\sqrt{\frac{2}{3}\frac{p_v - p_s}{\rho_f}} \tag{1}$$

$$R_c = F_{cond}\frac{3\alpha_v\rho_g}{R_B}\sqrt{\frac{2}{3}\frac{p_s - p_v}{\rho_f}} \tag{2}$$

Where α_{nuc} is the volume fraction of the nucleation sites, R_B is the bubble radius, p_v is the pressure in the bubble, p_s is the pressure in the liquid surrounding the bubble, ρ_f is the liquid density, F_{vap} is the empirical factor for the vaporization process, F_{cond} is the empirical factor for the condensation process, R_e is the vaporization rate per unit volume, and R_c is the condensation rate per unit volume. The model parameters in the above equation take the values: $\alpha_{nuc}=5\times10^{-4}$, $F_{vap}=50$, $F_{cond}=0.01$, and $R_B=1$ μm.

The inlet and outlet of the pump are the total pressure and bulk mass flow rate boundary conditions, respectively. The turbulence intensity I at the inlet is set to 5%, and I is specified as:

$$I = \frac{\hat{u}}{u_{avg}} \tag{3}$$

Where $\hat{u}$ is the root mean square of the velocity pulsation and u_{avg} is the average velocity.

The impeller part is built up as a rotating domain, and all walls are non-slip walls. The impeller wall roughness is set to 50 μm, the remaining components to 100 μm, and the components are linked by setting the interface. In unsteady simulation, verification of time step independence is required before the time step is set. Considering the analysis of the subsequent results, it is necessary to divide the 1/6 rotation of the impeller into 5 moments. Then the maximum value of the time step can only take the time taken to rotate the impeller by 15° without affecting the analysis of the results. Therefore, four sets of different time steps are formulated for the time required to rotate the impeller by 1°, 3°, 5°, and 15°, corresponding to 5.73×10^{-5} s, 1.72×10^{-4} s, 2.86×10^{-4} s, and 8.60×10^{-4} s, respectively. For the calculation, the flow rate of 66.2 m^3/h and the $NPSH_a$ of 4.7 m are used. The criterion for judging the independence of time step is to select the total volume of the vapor in the impeller at the same moment. Figure 3 displays the final result. As the time step gets smaller, the vapor volume tends to stabilize, as seen in Fig. 3. When the time step is

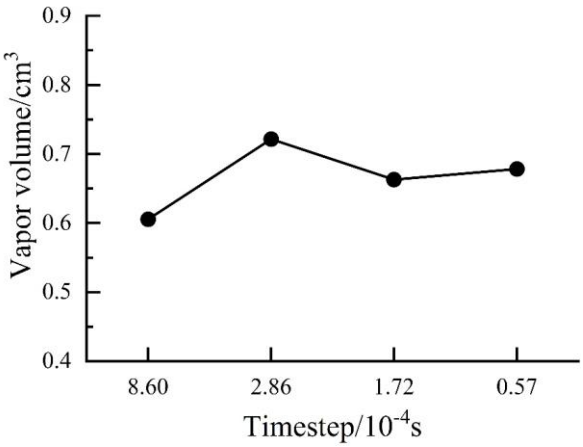

Fig. 3 Verification of time step independence

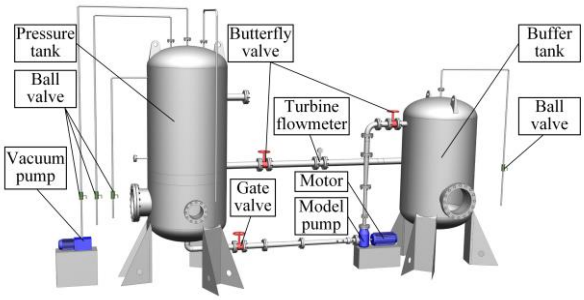

Fig. 4 Schematic of the test system

5.73×10^{-5} s, the time spent on the calculation is several times that of other options. As a result, the time step is set to 1.72×10^{-4} s, which ensures calculation accuracy while conserving computational resources. The overall time was set to 0.1649 s, which equates to 8 impeller spins, with the last 1/6th of a rotation used for the analysis. In order to accelerate the convergent process of the numerical calculation and lower the computational resource consumption, the steady simulation results are considered the initial flow field of the transient simulation.

2.2 Experimental Verification of Numerical Calculation Method

It is common practice to compare the consistency of the cavitation characteristic curves acquired from numerical calculations and experiments in order to confirm the accuracy of the simulation method for cavitation flow in centrifugal pumps (Rakibuzzaman et al., 2018). The closed test system depicted in Fig. 4 was used for the cavitation tests in this research. The medium used in the test system is water at a normal temperature. The model pump has a rated specific speed (n_s) of 132.2, a rated flow rate (Q_d) of 50.6 m^3/h, a rated head (H_d) of 20.2 m, a rated rotational speed (n) of 2910 r/min, a blade number (Z) of 6, a blade passing frequency (f_d) of 291 Hz, and a shaft frequency (f_0) of 48.5 Hz.

Figure 5 displays the cavitation characteristic curves for the pump at 1.3 Q_d and 1.0 Q_d, where H is the measured pump head, as determined by numerical calculations and experiments. The findings displayed in the image demonstrate

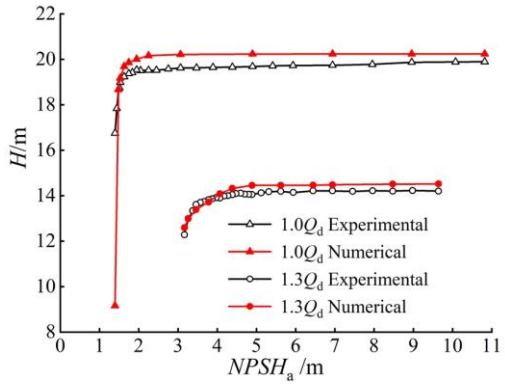

Fig. 5 Comparison of model pump test and numerical calculation of cavitation characteristics

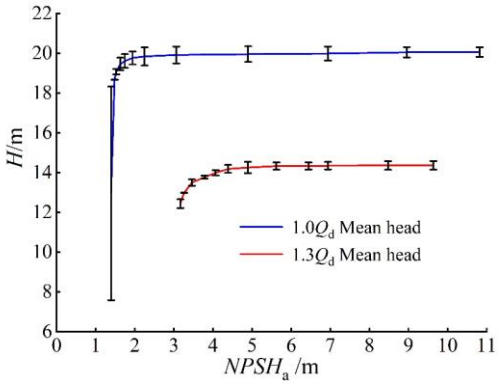

Fig. 6 Error analysis of test and numerical calculation of cavitation characteristics

that the cavitation characteristic curves derived using the two approaches are almost identical. Figure 6 shows the error bar analysis of the cavitation characteristics, with the solid line representing the average head. The results show that the maximum error occurs when $NPSH_a$ = 5.62 m, and 1.3 Q_d has a standard deviation of 5.37. The reason for the large error at this time is that a head fracture occurs, and a large number of vapors in the pump lead to an extremely complicated flow. As a result, simulating the real flow in the pump is more challenging. The maximum value of the standard deviation is 0.45 under the rest of the working conditions. The primary reason of the error is that factors such as the quantity of leakage at the wear ring were not taken into account in the numerical calculation (Lu, 2017). All of the errors are within acceptable limits, indicating that the numerical calculations are reliable.

3. RESEARCH ON THE TONGUE CAVITATION CHARACTERISTICS

According to our earlier research, high flows are more likely to cause tongue cavitation (Lu et al., 2022). Figure 7 illustrates the variation of the vapor bubble distribution at the tongue with a decrease in $NPSH_a$ at 1.3 Q_d, where vapors are represented by a bubble volume concentration of 10%. When the $NPSH_a$ is 5.62 m, the presence of smaller-scale vapors is observed in the area at the tongue upon magnification. As $NPSH_a$ begins to be reduced, the volume of the vapor at the tongue gradually increases. This is because when the $NPSH_a$ lowers, the region of the tongue below the vaporization pressure expands, further

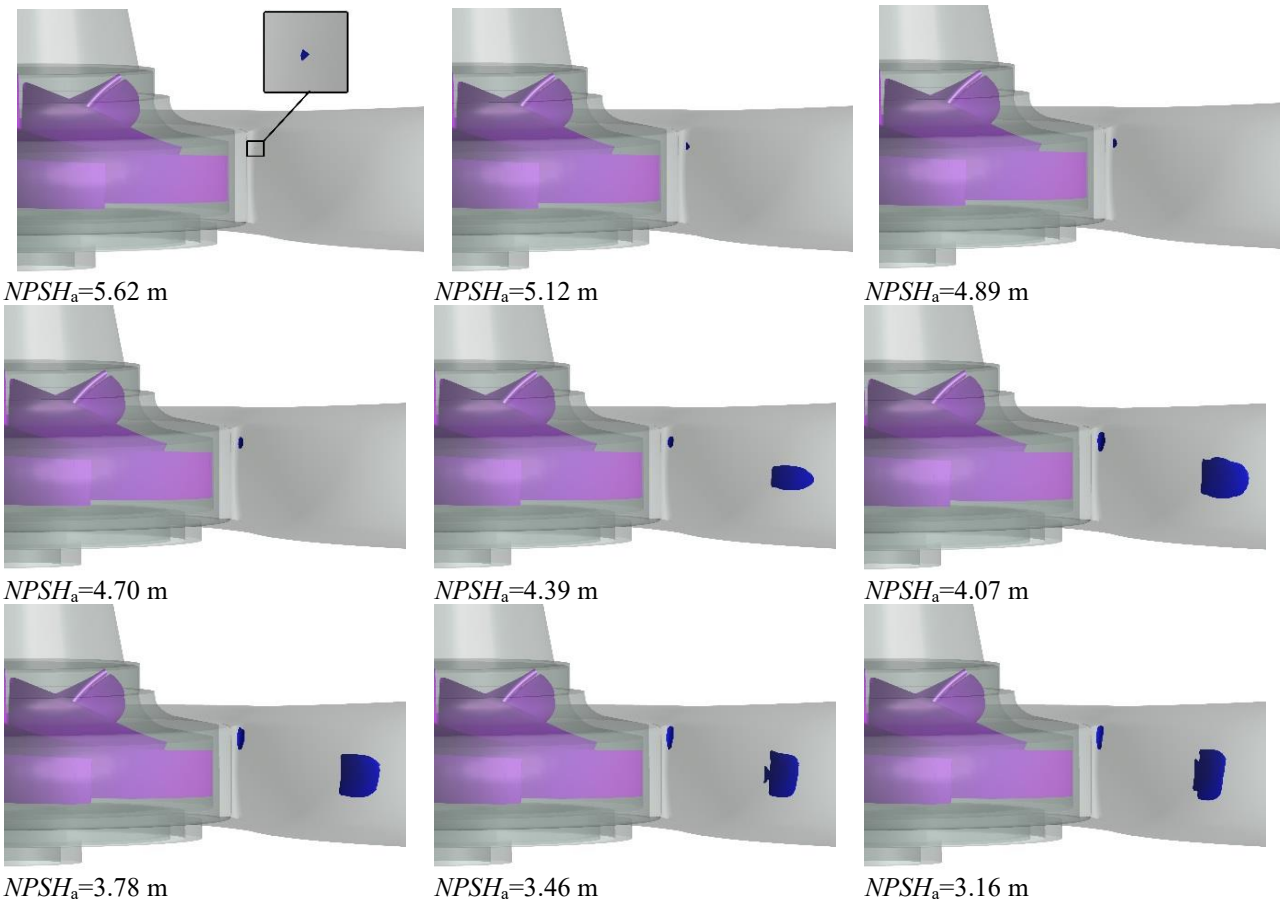

Fig. 7 Cavitation evolution at the tongue

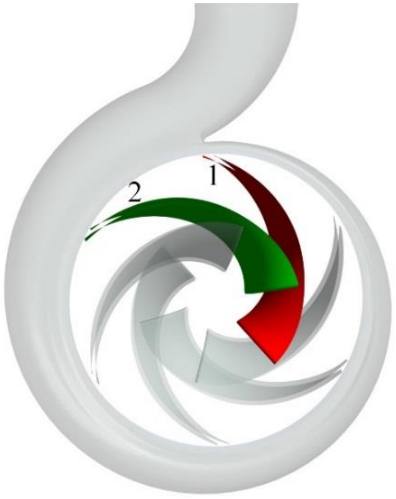

Fig. 8 Relative position of the blades

deteriorating cavitation. Cavitation was also observed at other locations within the diffusion tube at an $NPSH_a$ of 4.39m. The main reason for cavitation in this area is the high flow velocity in the diffusion tube at overload flow rate conditions, which causes the flow to break away from the wall in this area. Because of the effect of the wall, the fluid flow velocity near the wall is lower, resulting in the formation of a vortex at the wall downstream of the bend in the diffusion tube, where the pressure at the center of the vortex is generally lower. Thus, cavitation occurs. As $NPSH_a$ continues to fall below 3.78 m, no significant deterioration of tongue cavitation occurs. This phenomenon is inconsistent with the known development of cavitation within the impeller, the main cause of which is the special structure of the tongue. The cloud cavitation that occurs in the hydrofoil is experimentally demonstrated by the fact that the thickness of the cavity is directly controlled by the hydrofoil angle of attack (Ju et al., 2018). Due to the similarity between the tongue cavitation and the hydrofoil cavitation, we may conclude that the scale of the cavitation cloud at the tongue is controlled by the angle of attack. The flow conditions that the centrifugal pumps are running under have an impact on the angle of attack. The creation of localized low-pressure zones due to pressure loss induced by flow separation is the primary cause of tongue cavitation (Limbach & Skoda, 2017). Due to the work of the impeller, the pressure in the area of the diffuser tube where flow separation does not occur is always high. No clear pattern is observed for the cavitation occurring at another location in the diffusion tube as $NPSH_a$ decreases.

As an unsteady cavitation, the non-constant characteristics of the tongue cavitation process are closely linked to the periodic flow field generated by the rotational work of the impeller. Therefore, in order to find out the relationship between the non-constant characteristics of the tongue cavitation and the work of the blade, the position of the blades in the impeller is tracked by rendering the blade and numbering it to facilitate analysis, as shown in Fig. 8, where the red and green blades are numbered 1 and 2, respectively.

Figure 9 illustrates the evolution of the tongue cavitation with the work done by the impeller at Q =1.3 Q_d and $NPSH_a$ =4.07 m. The total time taken to rotate the impeller 1/6th of a revolution is defined as t. Splitting t into four periods of equal length is used to analyze the evolution of cavitation. The blade 1 is closest to the tongue at moment 0 t. The formation of a larger volume of cloud cavitation at the tongue at this point squeezes the nearby fluid while reducing the passable cross-sectional area of the fluid in the diffusion tube. At time t/4, Blade 2 starts to progressively approach the tongue, while Blade 1 has already departed. The previous cavity has now split into two smaller vapors. The position of one component of the vapor changes slightly, while the other half of the vapor travels downstream with the flow of the liquid. The movement of the vapor downstream affects the stability of the downstream flow field. The blades have moved further with the impeller rotation at t/2. The vapors formed during the previous separation remained partially attached to the tongue but were significantly smaller. The flow blockage in the diffusion tube was relieved. The other component

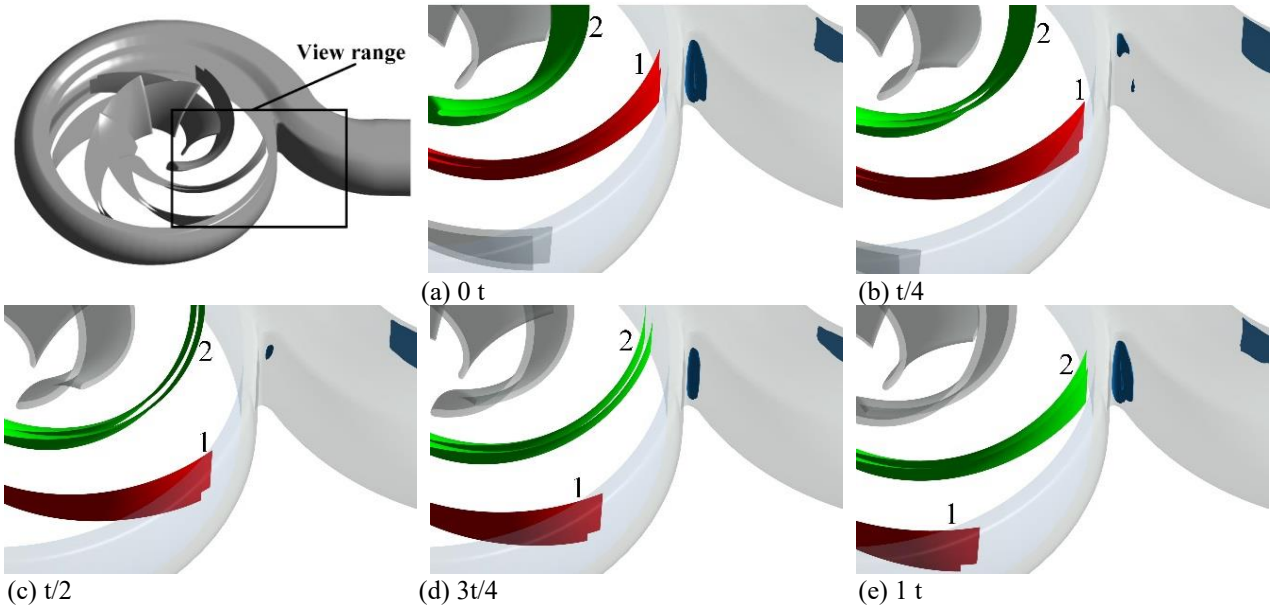

Fig. 9 Cavitation evolution at the tongue when $NPSH_a$=4.07 m and Q=1.3 Q_d

of the vapor that flows with the liquid is no longer observed. This is because the vapor moves downstream to high pressures, where it is compressed in volume and eventually collapses. At 3t/4, the cavity develops into the shape of a finger and is evenly distributed over the tongue as Blade 2 gets closer to the tongue. The blade 2 is again closest to the tongue at moment 1 t. At this point, the vapor grows into a bigger cavity with a structure that is essentially identical to that of the 0 t moment. A complete cycle is completed by the evolution of the tongue cavitation. The whole cycle of vapor shedding consists of development, shedding, and collapse. This result is in line with the experimental findings of Hu et al. (2020). It is obvious from the change of blade position and the process of vapor shedding that the time taken for the impeller to rotate 1/6 turn is the cavity shedding cycle.

To investigate the non-constant flow field near the tongue, Fig. 10 illustrates the distribution of the velocity vector in the flow field near the tongue in the mid-section of the impeller at different moments of t in the condition of 1.3 Q_d with an $NPSH_a$ of 4.07 m. The velocity magnitude of the fluid flow is indicated by different colors. The fluid has a tendency to travel along the tongue wall at 0 t after hit the tongue at a significant incidence angle. The Coanda Effect (Ahmed et al., 2017), which is the major cause of this occurrence, is caused by the fluid's viscosity. There is a risk of flow separation due to excessive wall curvature and high fluid velocity at the tongue. Flow separation can result in separation vortex. Typically, the pressure in the vortex's center is quite low, making it vulnerable to vortex cavitation. By observing the 0 t in Fig. 9, it is found out that a large-scale cavitation cloud exists at this time at the tongue. It is also observed that there is a large area of low velocity in the annular chamber of the volute located on the left of the figure. This phenomenon is attributed mainly to high flow conditions, where the incident angle of the fluid flow leads to the formation of a flow stagnation zone in the region (Zhu et al., 2020). The presence of a smaller-scale separation vortex a at the downstream position of the tongue is noticed and is suspected to be formed by the separation vortex shedding at the tongue in relation to the vapor shedding process. At t/4, the incoming flow at the tongue changes due to the rotation of the impeller, and the separation vortex b starts to move downstream. The adverse pressure gradient around the tongue leads to the creation of a re-entrant jet, which moves upstream by adhering to the tongue wall, thus cutting off the large-scale cavity at the tongue and leading to the shedding of the vapor downstream in Fig. 9. The separation vortex a also moves downstream, and the vortex scale decreases as it moves. At t/2, the flow separation is significantly weaker as the direction of the fluid flow changes, but the fluid velocity remains faster at the tongue due to the fluid bypassing the tongue. The separation vortex b moves further downstream than at the previous moment and causes a significant increase in the velocity of the fluid at the same section of the diffusion tube. This phenomenon is due to the fluid's continuity, so that the flow rate is constant through different sections of the diffusion tube. However, the flow velocity in the area where the vortex is located is low, so the flow velocity of the fluid in the same section as the vortex is significantly higher. Separation vortex a completely disappears, and the flow downstream restores smoothness. At 3t/4, the direction of the incoming flow at the tongue changes again, and the angle of attack begins to increase. Backflow occurs again near the tongue; some of the fluid is moving upstream along the wall, and a new separation vortex is formed, corresponding to the development of a vapor at the tongue in Fig. 9. The separating vortex b moves further downstream. At 1 t, with the change in incident angle, flow separation is already severe, separation vortex c is formed, and separation vortex b becomes significantly smaller in scale as it moves downstream. The separation vortex a forms at the tongue and subsequently sheds with the flow to a position downstream of the tongue, as seen by comparing the distribution of the velocity vector at 0 t and 1 t. The separation vortex shedding cycle is the time taken for 1/6th of a rotation of the impeller. Through observation of the flow in the rest of the diffusion tube during the shedding of the separating vortex, it can be found that the flow in the diffusion tube is not uniform. At various moments, the cross section where the separating vortex is located has a higher maximum fluid velocity than other places. Flow blockage always occurs at the tongue, but it can manifest itself to varying degrees at different times.

The formation and collapse of vapors lead to an extremely complex flow at the tongue. The unsteady simulation of single-phase flow in the condition of 1.3 Q_d with an $NPSH_a$ of 4.07 m is carried out without a cavitation model. The effect of cavitation on the flow characteristics at the tongue is discussed by comparing the flow with the cavitation model. Figures 11 and 12 show the streamline and pressure distributions at different moments at the tongue with and without the addition of the cavitation model, respectively. The previous analysis shows that the periodicity of the flow field makes it essentially the same at 1 t as it is at 0 t. Therefore, Figs 11, 12, and 13 only show the results for the first four moments, with no further elaboration of the results for the 1 t moment. By comparing the pressure distributions of the two flow cases, it can be found that the overall pattern of pressure distribution and size of the flow field do not differ much, but the pressure distribution near the tongue is obviously different. In single-phase flow, the pressure at the tongue is always low and fluctuates within a certain range as the direction of incoming flow changes, while the pressure in the downstream region does not change significantly. In the cavitation flow, the low pressure region near the tongue is larger, which is due to the creation of vapors that complicate the flow and intensify the dissipation of energy. When the pressure distributions in the cavitation flow are compared at different times, it is discovered that the pressure values in the low pressure region gradually increase as they move downstream. As was discussed above, this phenomenon is connected to the vapor shedding process. The vapor volume becomes smaller and smaller during shedding, and it eventually collapses. During the movement of the low-pressure area, the pressure gradually rises and finally recovers to the same value as in other downstream areas. By comparing the streamline distribution in the two flow cases, it can be found that there is a shedding vortex at the tongue in the

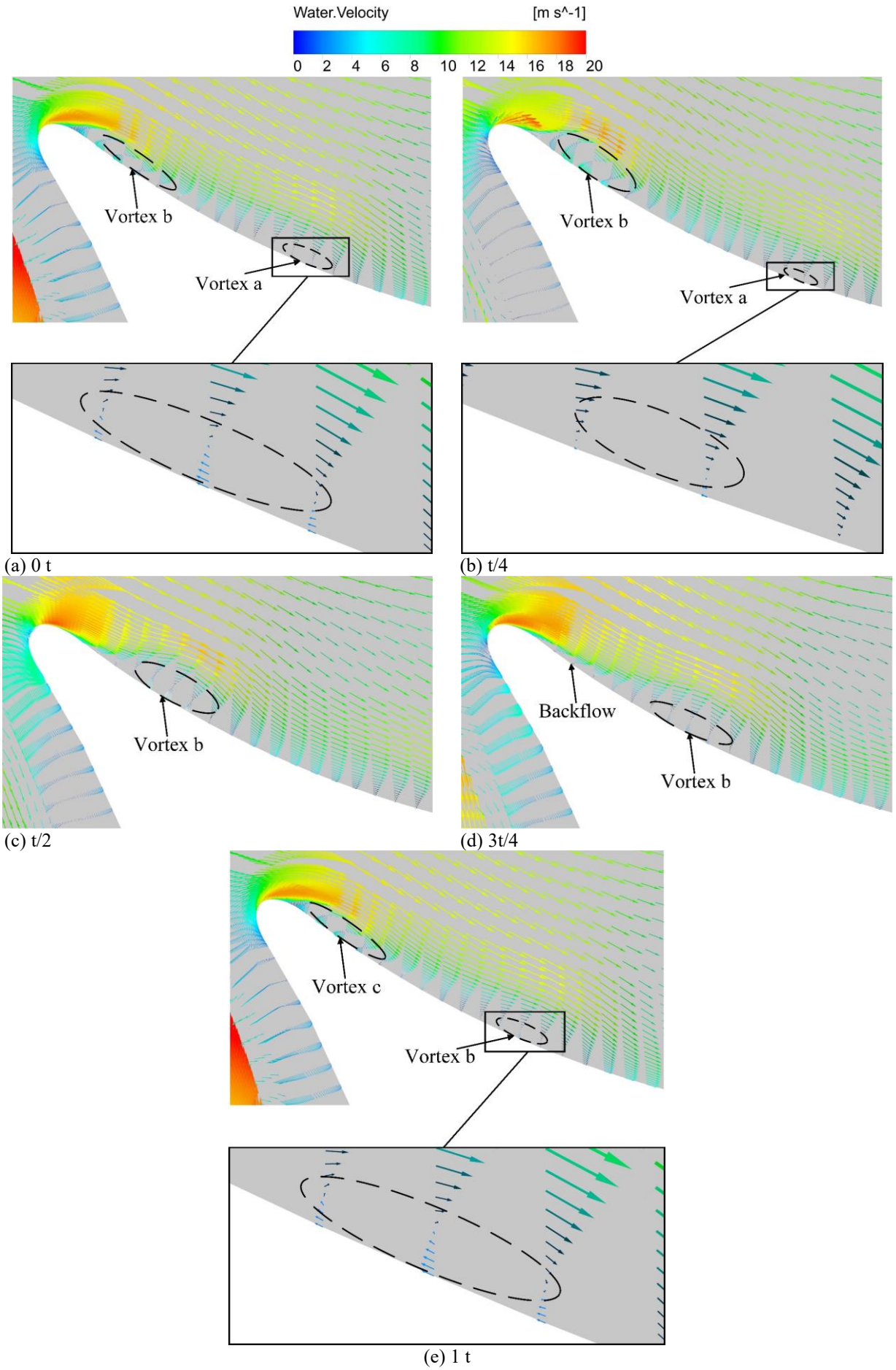

Fig. 10 Velocity vector distribution at different time of the tongue

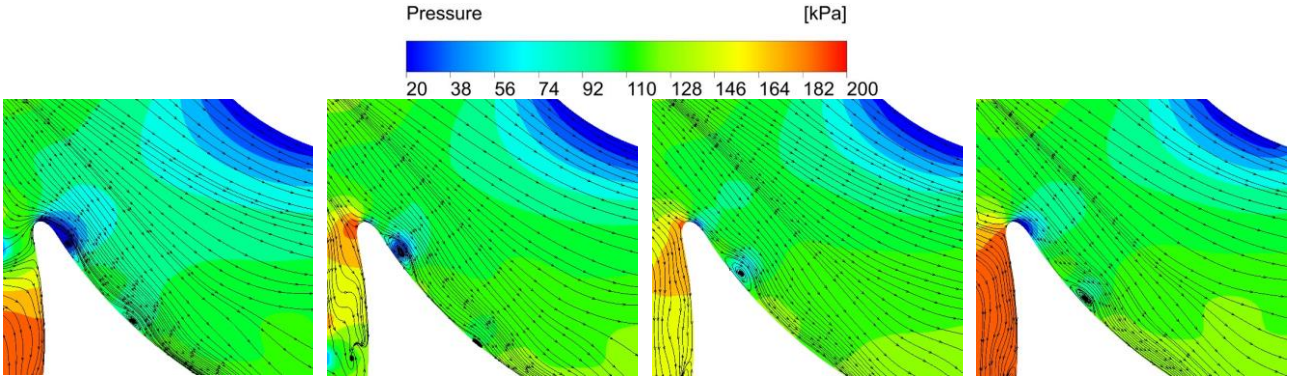

(a) 0 t (b) t/4 (c) t/2 (d) 3t/4

Fig. 11 Streamlines and pressure contours at different moments at the tongue when the cavitation model was added

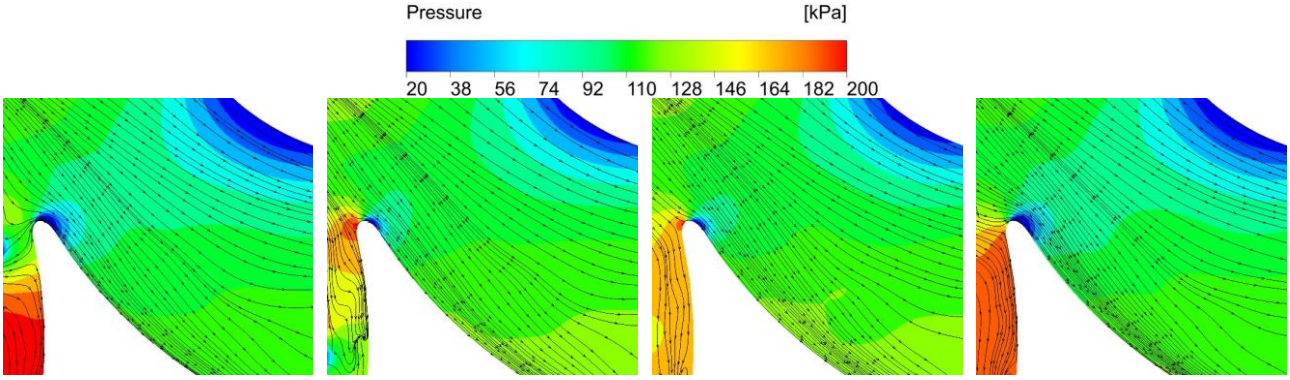

(a) 0 t (b) t/4 (c) t/2 (d) 3t/4

Fig. 12 Streamlines and pressure contours at different moments at the tongue when the cavitation model was not added

cavitation flow, whereas no vortex is observed at the tongue in the single-phase flow. The main cause of vortex formation here is related to vapors. The vapors attached to the tongue squeeze the fluid, causing a separation of the fluid from the tongue wall. This phenomenon is similarly found in a circular cylinder wake, where the creation of vapor squeezes the fluid and shifts the stagnation point of flow separation forward. A certain curvature exists on the downstream wall, thus avoiding flow separation in the context of single-phase flow.

The shedding process of tongue cavitation and the shedding process of separation vortex are closely related. To further analyze the link between the pattern of vorticity distribution near the tongue and the process of cavitation development, the relative vorticity transport equation is introduced (Zhao et al., 2014):

$$\frac{D\omega_r}{Dt}=(\omega_r\cdot\nabla)V-\omega_r(\nabla\cdot V)+\frac{\nabla\rho_f\times\nabla p}{\rho_f^{\ 2}}+\nu\nabla^2V \tag{4}$$

Where ω_r is relative vorticity vector, V is relative velocity vector, and ν is dynamic viscosity.

The right-hand side of the above equation shows, in order, the relative vortex stretching term (RVS), which represents the change in vorticity due to the velocity gradient of the flow field; the relative vortex dilatation term (RVD), which represents the change in vorticity as caused by the change in volume of a fluid microcluster; the baroclinic torque term (BART), which represents the change in vorticity as caused by non-parallel pressure gradient and density gradient; and the viscous diffusion term (VISD), which represents the viscous diffusion effect of the vorticity (Sun, 2020). As the VISD term has significantly less influence on flow in cavitation flow than the other terms (Liu et al., 2019), only the first three are analyzed in relation to the vapor volume fraction (α).

Figure 13 illustrates the distribution of the α, RVS term, RVD term and BART term in the vicinity of the tongue. By comparing the values of the different terms and the range of high value areas, it can be found that the values of the RVS and RVD terms are much larger than those of the BART term, with the RVS term having a wider range of high value areas than the RVD term. According to the distribution of the RVS term at different moments, the main area of distribution is where the vapor is located, and it develops along the wall of the tongue towards the sides. Along with the shedding of vapors, part of the high value region of the RVS term moves downstream. This is attributable to the large velocity gradient at the tongue, which causes stretching and bending of the vortex lines. In turn, this can cause stretching of the cavity. The high value region of the RVD term is mainly located in the cavity and downstream of it.

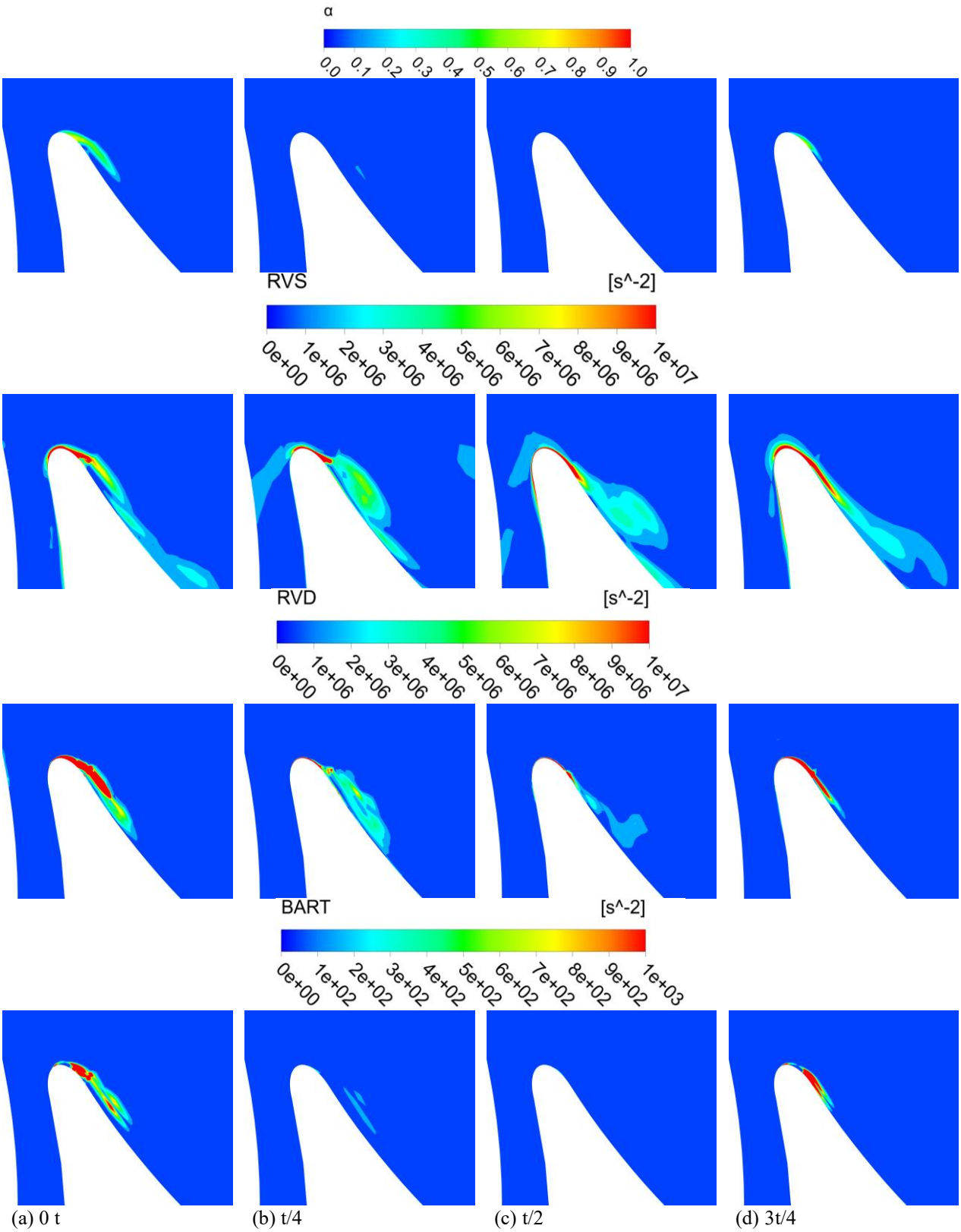

Fig. 13 Contours of *α*, RVS, RVD and BART at different times at the tongue

It decreases as the vapor is shed. The value of this term starts to rise again when the vapor is formed again at 3t/4. This is because the RVD term mainly describes the change in vapor volume, which is evident during the development of cavitation. During vapor shedding, there were consistently high values of the RVS and RVD terms in the region downstream of the vacuole, suggesting that these two terms promote vapor shedding. Given that the BART term is used to describe the abrupt change in density, which is caused by the change in pressure, it is comparable to the distribution of the α. At the vapor-liquid boundary, this frequently happens quite intensely. The distribution of the BART term is not clearly observed at t/2, as the vapor is known to collapse at that moment according to the distribution of the α and Fig. 9(c).

4. CONCLUSION

This work explores the unsteady flow characteristics of tongue cavitation, which have received less attention from scholars, after confirming the accuracy of the numerical method, mostly using numerical calculations. In addition, by introducing the vorticity transport equation, the vortex features of the tongue cavitation flow are examined. Finally, the following key findings are deduced:

(1) After the occurrence of the tongue cavitation of the centrifugal pump, it gradually deteriorates as the $NPSH_a$ decreases. However, when $NPSH_a$ is reduced to 3.78 m, it no longer changes significantly with the decrease of the $NPSH_a$.

(2) At the tongue, the extrusion of fluid by the vapor promotes the formation of the separation vortex, and the re-jet flow caused by the separation vortex leads to vapor shedding. The period of cavitation shedding is consistent with the period of vortex shedding.

(3) The relative vortex stretching term and the relative vortex dilatation term dominate vapor shedding by controlling the variation of vorticity, while the baroclinic torque term affects the variation of vorticity at the vapor-liquid interface. The magnitude of this variation is much smaller than the first two terms.

(4) This study focuses on cavitation flow at the tongue, which has not yet attracted much attention, from the perspectives of deterioration of cavitation, shedding of vapors and vortices, and distribution of pressure and vorticity. Some characteristics of tongue cavitation flow are proposed, which lays the foundation for more in-depth research on tongue cavitation in the future. Due to the limitation of experimental conditions, this study involves no visualization studies of the related contents. More scientifically significant findings can be obtained by conducting visualization studies on related contents in the future.

ACKNOWLEDGEMENTS

This work was financially supported by the National Natural Science Foundation of China (Grant NO. 52009115).

CONFLICT OF INTEREST

The authors declare there is no conflict.

AUTHORS CONTRIBUTION

Z. Y. Luo: Formal analysis, Software, Writing-original draft; **Y. Feng**: Methodology, Writing – review & editing; **X. Y. Sun**: Data curation, Validation; **Y. Gong**: Supervision, Investigation; **J. X. Lu**: Funding acquisition, Experiment; **X. W. Zhang**: Experiment.

REFERENCES

Ahmed, R. I., Abu Talib, A. R., Rafie, A. S. M., & Djojodihardjo, H. (2017). Aerodynamics and flight mechanics of mav based on coanda effect. *Aerospace Science and Technology*, *62*, 136-147. https://doi.org/10.1016/j.ast.2016.11.023

Al-Obaidi, A. R. (2019). Investigation of effect of pump rotational speed on performance and detection of cavitation within a centrifugal pump using vibration analysis. *Heliyon*, *5*(6), e01910. https://doi.org/10.1016/j.heliyon.2019.e01910

Al-Obaidi, A. R. (2023a). Effect of different guide vane configurations on flow field investigation and performances of an axial pump based on cfd analysis and vibration investigation. *Experimental Techniques*, 1-20. https://doi.org/10.1007/s40799-023-00641-5

Al-Obaidi, A. R. (2023b). Experimental diagnostic of cavitation flow in the centrifugal pump under various impeller speeds based on acoustic analysis method. *Archives of Acoustics*, *48*(2), 159-170. https://doi.org/10.24425/aoa.2023.145234

Al-Obaidi, A. R., & Alhamid, J. (2023). Investigation of the main flow characteristics mechanism and flow dynamics within an axial flow pump based on different transient load conditions. *Iranian Journal of Science and Technology-Transactions of Mechanical Engineering*, 1-19. https://doi.org/10.1007/s40997-022-00586-x

Al-Obaidi, A. R., & Qubian, A. (2022). Effect of outlet impeller diameter on performance prediction of centrifugal pump under single-phase and cavitation flow conditions. *International Journal of Nonlinear Sciences and Numerical Simulation*, *23*(7-8), 1203-1229. https://doi.org/10.1515/ijnsns-2020-0119

Astolfi, J. A., Dorange, P., & Tomas, I. C. (2000). An experimental investigation of cavitation inception and development on a two-dimensional eppler hydrofoil. *Journal of Fluids Engineering-Transactions of the ASME*, *122*(1), 164-174. https://doi.org/10.1115/1.483239

Bachert, R., Stoffel, B., & Dular, M. (2010). Unsteady cavitation at the tongue of the volute of a centrifugal pump. *Journal of Fluids Engineering-Transactions of the Asme*, *132*(6), 061301. https://doi.org/10.1115/1.4001570

Bakir, F., Rey, R., Gerber, A. G., Belamri, T., & Hutchinson, B. (2004). Numerical and experimental investigations of the cavitating behavior of an inducer. *International Journal of Rotating Machinery*, *10*, 690740. https://doi.org/10.1155/S1023621X04000028

Dular, M., & Bachert, R. (2009). The issue of strouhal number definition in cavitating flow. *Strojniski Vestnik-Journal of Mechanical Engineering*, *55*(11), 666-674.

Dular, M., Bachert, R., Stoffel, B., & Sirok, B. (2005). Experimental evaluation of numerical simulation of cavitating flow around hydrofoil. *European Journal of Mechanics B-Fluids*, *24*(4), 522-538. https://doi.org/10.1016/j.euromechflu.2004.10.004

Foeth, E. J., Van Doorne, C. W. H., Van Terwisga, T., & Wieneke, B. (2006). Time resolved piv and flow visualization of 3d sheet cavitation. *Experiments in Fluids*, *40*(4), 503-513. https://doi.org/10.1007/s00348-005-0082-9

Foeth, E. J., Van Terwisga, T., & Van Doorne, C. (2008). On the collapse structure of an attached cavity on a three-dimensional hydrofoil. *Journal of Fluids Engineering-Transactions of the Asme*, *130*(7), 071303. https://doi.org/10.1115/1.2928345

Folden, T. S., & Aschmoneit, F. J. (2023). A classification and review of cavitation models with an emphasis on physical aspects of cavitation. *Physics of Fluids*, *35*(8), 081301. https://doi.org/10.1063/5.0157926

Hattori, S., & Kishimoto, M. (2008). Prediction of cavitation erosion on stainless steel components in centrifugal pumps. *Wear*, *265*(11-12), 1870-1874. https://doi.org/10.1016/j.wear.2008.04.045

Hu, Q. X., Yang, Y., Shi, W. D., Cao, W. D., & Shi, Y. S. (2021). Cavitating flow in the volute of a centrifugal pump at flow rates above the optimal condition. *Journal of Marine Science and Engineering*, *9*(4), 446. https://doi.org/10.3390/jmse9040446

Hu, Q., Yang, Y., & Cao, W. (2020). Computational analysis of cavitation at the tongue of the volute of a centrifugal pump at overload conditions. *Advances in Production Engineering & Management*, *15*(3), 295-306. https://doi.org/10.14743/apem2020.3.366

Ji, B., Luo, X. W., Wu, Y. L., Peng, X. X., & Duan, Y. L. (2013). Numerical analysis of unsteady cavitating turbulent flow and shedding horse-shoe vortex structure around a twisted hydrofoil. *International Journal of Multiphase Flow*, *51*, 33-43. https://doi.org/10.1016/j.ijmultiphaseflow.2012.11.008

Jiang, J., Li, Y. H., Pei, C. Y., Li, L. L., Fu, Y., Cheng, H. G., & Sun, Q. Q. (2019). Cavitation performance of high-speed centrifugal pump with annular jet and inducer at different temperatures and void fractions. *Journal of Hydrodynamics*, *31*(1), 93-101. https://doi.org/10.1007/s42241-019-0011-7

Ju, D. M., Xiang, C. L., Wang, Z. Y., Li, J., & Xiao, N. X. (2018). Flow structures and hydrodynamics of unsteady cavitating flows around hydro-foil at various angles of attack. *Journal of Hydrodynamics*, *30*(2), 276-286. https://doi.org/10.1007/s42241-018-0033-6

Kravtsova, A. Y., Markovich, D. M., Pervunin, K. S., Timoshevskiy, M. V., & Hanjalic, K. (2014). High-speed visualization and piv measurements of cavitating flows around a semi-circular leading-edge flat plate and naca0015 hydrofoil. *International Journal of Multiphase Flow*, *60*, 119-134. https://doi.org/10.1016/j.ijmultiphaseflow.2013.12.004

Launder, B. E., & Spalding, D. B. (1974). The numerical computation of turbulent flows. *Computer Methods in Applied Mechanics and Engineering*, *3*, 269-289.

Limbach, P., & Skoda, R. (2017). Numerical and experimental analysis of cavitating flow in a low specific speed centrifugal pump with different surface roughness. *Journal of Fluids Engineering-Transactions of the Asme*, *139*(10), 101201. https://doi.org/10.1115/1.4036673

Liu, M., Tan, L., & Cao, S. L. (2019). Cavitation-vortex-turbulence interaction and one-dimensional model prediction of pressure for hydrofoil ale15 by large eddy simulation. *Journal of Fluids Engineering-Transactions of the Asme*, *141*(2), 021103. https://doi.org/10.1115/1.4040502

Liu, Y. W. (2021). *Study on the influent of non-uniform inflow on performance of centrifugal pump and optimization*. [Master's thesis, Xian University of Technology]. Xian, China. [in Chinese].

Lu, J. X. (2017). *Investigation on the unsteady dynamic characteristics and its mechanism induced by cavitation in a centrifugal pump*. [PhD. thesis, Jiangsu University]. Zhenjiang, China. [in Chinese].

Lu, J. X., Gong, Y., Li, L. H., Liu, X. B., Kan, N. Q., & Zhang, F. (2023). Research of the vibration induced by cavitation in a centrifugal pump under part load condition. *Physics of Fluids*, *35*(4), 045144. https://doi.org/10.1063/5.0150364

Lu, J. X., Liu, X. B., Zeng, Y. Z., Zhu, B. S., Hu, B., & Hua, H. (2020). Investigation of the noise induced by unstable flow in a centrifugal pump. *Energies*, *13*(3), 589. https://doi.org/10.3390/en13030589

Lu, J. X., Liu, X. B., Zeng, Y. Z., Zhu, B. S., Hu, B., Yuan, S. Q., & Hua, H. (2019). Detection of the flow state for a centrifugal pump based on vibration. *Energies*, *12*(16), 3066. https://doi.org/10.3390/en12163066

Lu, J. X., Luo, Z. Y., Chen, Q., Liu, X. B., & Zhu, B. S. (2022). Study on pressure pulsation induced by cavitation at the tongue of the volute in a centrifugal pump. *Arabian Journal for Science and Engineering*, *47*(12), 16033-16048. https://doi.org/10.1007/s13369-022-06829-y

Mandhare, N. A., Karunamurthy, K., & Ismail, S. (2019). Compendious review on "Internal flow physics and minimization of flow instabilities through design modifications in a centrifugal pump". *Journal of Pressure Vessel Technology-Transactions of the Asme*, *141*(5), 051601. https://doi.org/10.1115/1.4043383

Park, S., & Rhee, S. H. (2013). Numerical analysis of the three-dimensional cloud cavitating flow around a twisted hydrofoil. *Fluid Dynamics Research*, *45*(1), 015502. https://doi.org/10.1088/0169-5983/45/1/015502

Pham, T. M., Larrarte, F., & Fruman, D. H. (1999). Investigation of unsteady sheet cavitation and cloud cavitation mechanisms. *Journal of Fluids Engineering-Transactions of the ASME*, *121*(2), 289-296. https://doi.org/10.1115/1.2822206

Rakibuzzaman, M., Kim, K., & Suh, S. H. (2018).

Numerical and experimental investigation of cavitation flows in a multistage centrifugal pump. *Journal of Mechanical Science and Technology*, *32*(3), 1071-1078. https://doi.org/10.1007/s12206-018-0209-6

Shi, W. C., Atlar, M., Rosli, R., Aktas, B., & Norman, R. (2016). Cavitation observations and noise measurements of horizontal axis tidal turbines with biomimetic blade leading-edge designs. *Ocean Engineering*, *121*, 143-155. https://doi.org/10.1016/j.oceaneng.2016.05.030

Si, Q. R., Yuan, S. Q., Li, X. J., Yuan, J. P., & Lu, J. X. (2014). Numerical simulation of unsteady cavitation flow in the casing of a centrifugal pump. *Transactions of the Chinese Society for Agricultural Machinery*, *45*(05), 84-90. [in Chinese]. https://doi.org/10.6041/j.issn.1000-1298.2014.05.013

Sun, W. H. (2020). *Research on the transient characteristics of startup process and cavitation under partial load in a centrifugal pump*. [Master's thesis, Shandong University of Science and Technology]. Qingdao, China. [in Chinese].

Tan, L., Zhu, B. S., Cao, S. L., Wang, Y. C., & Wang, B. B. (2014). Influence of prewhirl regulation by inlet guide vanes on cavitation performance of a centrifugal pump. *Energies*, *7*(2), 1050-1065. https://doi.org/10.3390/en7021050

Xue, M. X. (2012). *Investigation on cavitation mechanism and suppression method close to an afterburning fuel pump casing tongue*. [PhD. thesis, Tsinghua University]. Beijing, China. [in Chinese].

Xue, M. X., & Piao, Y. (2012). Numerical simulation on separation control by filleting casing tongue of after-burning fuel pump. *Journal of Aerospace Power*, *27*(12), 2799-2804. https://doi.org/10.13224/j.cnki.jasp.2012.12.003

Yuan, J. P., Hou, J. S., Fu, Y. X., Hu, J. W., Zhang, H. Y., & Shen. C. D. (2018). A study on the unsteady characteristics of the backflow votex cavitation in a centrifugal pump. *Journal of Vibration and Shock*, *37*(16), 24-30. [in Chinese]. https://doi.org/10.13465/j.cnki.jvs.2018.16.004

Zhao, Y., Wang, G. Y., & Huang, B. (2014). Vortex dynamic analysis of unsteady cavitating flows around a hydrofoil. *Journal of Drainage and Irrigation Machinery Engineering*, *32*(08), 645-651. [in Chinese]. https://doi.org/10.3969/j.issn.1674-8530.13.1020

Zhou, H. L., Cao, G. Y., Chen, X., Zhang, Y. Q., & Cang, Y. G. (2023). A study on the thermal properties of oil-film viscosity in squeeze film dampers. *Lubricants*, *11*(4), 163. https://doi.org/10.3390/lubricants11040163

Zhu, X. Y., Lai, F., Xie, C. C., Li, G. J., & Romuald, S. (2020). Experimental and numerical studies on the rotor-stator interaction of a centrifugal pump. *Journal of Harbin Engineering University*, *41*(08), 1176-1183. [in Chinese]. https://doi.org/10.11990/jheu.201904005